Nanoscale

# Improvement of coloration properties of Ag deposition-based plasmonic EC device by precise control of shape and density of deposited Ag nanoparticles



| | |
|---|---|
| Journal: | *Nanoscale* |
| Manuscript ID | NR-ART-07-2020-005196.R1 |
| Article Type: | Paper |
| Date Submitted by the Author: | 30-Sep-2020 |
| Complete List of Authors: | Kimura, Shunsuke; Chiba University, Graduate School of Engineering; Research Fellow of Japan Society for the Promotion of Science<br>Sugita, Tomoko; Chiba University, Graduate School of Engineering<br>Nakamura, Kazuki; Chiba University, Graduate School of Engineering<br>Kobayashi, Norihisa; Chiba University, Graduate School of Engineering |
| | |

ARTICLE

# Improvement of coloration properties of Ag deposition-based plasmonic EC device by precise control of shape and density of deposited Ag nanoparticles

Received 00th January 20xx,
Accepted 00th January 20xx

DOI: 10.1039/x0xx00000x

Shunsuke Kimura[a,b], Tomoko Sugita[a], Kazuki Nakamura[a], Norihisa Kobayashi*[a]

Ag nanoparticles exhibit various colors depending on their localized surface plasmon resonance (LSPR). Based on this phenomenon, Ag deposition-based electrochromic devices can represent various optical states in a single device such as the three primary colors (cyan, magenta, and yellow), silver mirror, black and transparent. A control of the morphology of Ag nanoparticles can lead to dramatic changes in color, as their size and shape influence the LSPR band. In this research, we focused on the diffusion rate of $Ag^+$ ion when Ag nanoparticles are electrochemically deposited. Consequently, well-isolated Ag nanoparticles were obtained due to slow growth rate by using an electrolyte with a low concentration of $Ag^+$ ions, resulting in an improvement in the color quality of cyan and magenta. Additionally, spherical Ag nanoparticles were deposited in the same device by optimizing the voltage application conditions, which represented yellow and green colors. In particular, green coloration is a unique phenomenon because it can appear by the combination of two absorption peaks of LSPR. As a result of investigating the finite-difference time-domain method, it was observed that the LSPR band in the long wavelength region was originated from the effects of the connection between Ag particles.

## 1. Introduction

Because the color and optical properties of materials reflect their electronic state, it is possible to reversibly control these properties by controlling the electronic state of the material through a reduction and oxidation (redox) reaction. This phenomenon is referred to as electrochromism (EC), which is expected to have a practical use for display devices, including electrochromic paper (E-paper) or smart windows[1,2]. EC displays have various advantages such as simple structure, large viewing angle, low power consumption, high visibility under sunlight, image retention property without electric power and color variation compared to conventional systems such as liquid-crystal display with backlight or organic light-emitting diodes[3–6]. Smart windows utilizing EC technology can maintain a comfortable environment in a room or inside a car in terms of brightness and temperature. In addition, smart windows will become promising candidates for energy-saving devices, contributing to reduced power consumption of air-conditioners[7–10]. In particular, considering the EC application to display devices, achieving multicolors with a single material or a single cell is desired. With regard to multicolor EC devices, the conventional approach is to use EC materials capable of multiple redox reactions related to color change, such as conductive polymers[11,12] and small organic molecules[6,13,14]. However, the stabilities of these highly oxidized or reduced states are not usually enough. Therefore, it is difficult to maintain a certain color under a high voltage and to satisfy adequate cycle stability. Some inorganic materials such as transition metal oxides[15–21], prussian blue[22–24] and prussian blue analogs[25–27] are also known to exhibit EC and have been used in practical applications, for instance smart windows. Prussian blue is a typical example of a mixed valence compound. The colored states of prussian blue or its analogs are based on the intervalence charge transfer between metal atoms with different valences or two species of metal atoms. The disappearance and appearance of intervalence charge transfer can be controlled by applying an external potential, leading to a reversible color-changing reaction. These redox reactions usually accompany insertion and de-insertion of cations with a small ionic radius, such as $H^+$, $Li^+$, and $K^+$, for the crystal lattice. This EC reaction has favorable cycle stability; however, as the optical states are based on changing the valences of metal atoms in the crystal lattice, multicoloration by a single material is limited.

Although there are commonly known organic and inorganic EC materials, as the above-mentioned, our interest is a novel type of EC material based on electrochemical deposition and dissolution of metals such as Ag[28–32], Bi[33] and Cu[34]. In this system, metal nanoparticles or films are formed on the transparent conductive electrode by the reduction of metal cations contained in the electrolyte solution, and these deposits modulate the color or reflection of the devices. In particular, we have reported EC devices based on deposition and dissolution of Ag that achieved six optical states in a single device (the three primary colors cyan, magenta and yellow, and silver mirror, black and transparent)[35–40]. The underlying mechanism of the achievement of such multicoloration was based on controlling the morphology of electrodeposited Ag nanoparticles on transparent electrodes. The EC material, i.e. gel electrolyte containing $Ag^+$ ions, was sandwiched by a pair of Indium tin oxide (ITO) electrodes: a flat ITO and an ITO particle modified electrode. The default state of the device was transparent, whereas applying a negative voltage to the electrode caused the electrodeposition of Ag

[a] Graduate School of Engineering, Chiba University, 1-33, Yayoi-cho, Inage-ku, Chiba, 263-8522, Japan. E-mail: koban@faculty.chiba-u.jp; Tel: +81-43-290-3458; Fax: +81-43-290-3457.
[b] Research Fellow of Japan Society for the Promotion of Science.

on its surface. It is noteworthy that this EC device can change its color based on simple electrochemical deposition and dissolution of Ag, thus achieving considerable cycle stability[35]. Moreover, multiple optical states can also be successfully achieved. Chromatic colors such as cyan, magenta and yellow are due to absorption by localized surface plasmon resonance (LSPR) enhanced by deposited Ag nanoparticles. The LSPR band is known to change its absorption wavelength depending on the size and shape of nanoparticles[41–43]. Therefore, dramatic changes in color are achieved by manipulating these bands.

For this purpose, the "voltage-step method" was applied to a Ag deposition-based EC device to obtain multiple colors by shifting the LSPR band. In this method, two different voltages are successively applied (Fig. S1): the first voltage $V_1$ is applied for a very short time $t_1$ to initiate the Ag nucleation, and the second voltage $V_2$ is applied for a time $t_2$ to promote growth of the Ag nuclei. As $V_2$ is more positive than the nucleation voltage, further nucleation is no longer possible during $t_2$[44,45]. Therefore, the Ag nanoparticles growth and the resultant device color can be controlled by changing $t_2$.

In our previous study, three chromatic colors (magenta, cyan and yellow) were successfully observed in the Ag deposition-based EC device by applying the voltage-step method[37,39]. When Ag nanoparticles were electrodeposited on the flat ITO electrode, anisotropic Ag nanoparticles were obtained to express magenta and cyan color. In contrast, to obtain a yellow color, Ag nanoparticles should be deposited on the rough ITO particle-modified electrode. In the yellow state, well-isolated fine spherical nanoparticles were formed on the modified electrode.

Various coloration abilities or vivid coloration on the EC device are required for practical applications such as displays and smart windows. On the Ag deposition-based EC device, the morphology of the Ag deposits, which significantly affect their colors, was expected to dramatically change by the composition of the electrolyte, particularly the concentration of $Ag^+$ ions or the voltage application method. In this study, the composition of the EC solution and the condition of step voltage application were optimized. As a result, more vivid cyan and magenta were successfully achieved in the Ag deposition-based multicolor EC device. Additionally, a green color representation was newly achieved as well as a yellow color in the same composition. Although, the previous study, the yellow color was only obtained on the rough ITO particle-modified electrode[37]. In this study, four chromatic colors (cyan, magenta, yellow and green) were successfully achieved on a flat ITO electrode, that is, the EC device was the simplest structure of two flat ITO electrodes and the sandwiched EC solution. Moreover, all chromatic colors in this device can appear on only one side of the flat ITO electrode, unlike the previously reported device. This novel phenomenon of yellow coloration on the flat ITO electrode is considerably interesting and discussed in detail in this study. To discuss the relationship between the morphologies of the electrodeposited Ag nanoparticles and the device colors, such as cyan, magenta, yellow or green, we performed microscopic analyses using field emission scanning electron microscopy (FE-SEM) and atomic force microscopy (AFM), and finite-difference time-domain (FDTD) calculation for the Ag nanoparticle models.

## 2. Experimental Procedures

### 2.1. Materials

Silver(I) nitrate ($AgNO_3$, Kanto Chemical Co. Inc.) and copper (II) chloride ($CuCl_2$, Kanto Chemical Co. Inc.) were used as received. Dimethyl sulfoxide (DMSO, Sigma Aldrich Japan) was used as solvent. Lithium bromide (LiBr, Kanto Chemical Co. Inc.) was used as the supporting electrolyte without further purification. Polyvinyl butyral (PVB, Mw = 5.0-6.0 × $10^4$, Kuraray Co. Ltd.) was used as a host polymer for electrolyte gelation. The ITO electrode (<10 Ω/□) was used after adequate washing.

### 2.2. Preparation of the EC electrolyte

The gel electrolyte for the electrochromic device was prepared as follows: 10, 50, and 150 mM of $AgNO_3$ as electrochromic material, five equivalents of LiBr in the molar ratio to $AgNO_3$ (i.e., 50, 250, and 750 mM) as supporting electrolyte, and 10 mM of $CuCl_2$ as electrochemical mediator were dissolved in DMSO. Subsequently, 10 wt.% of PVB as host polymer was mixed into the DMSO-based electrolyte solution.

### 2.3. Fabrication of the EC device

The EC device was fabricated by sandwiching a PVB-based gel electrolyte between a pair of flat ITO electrodes, maintaining an inner area of 1 $cm^2$ and an inter-electrode distance of 500 μm, using a Teflon spacer hollowed out in 1 cm × 1 cm.

### 2.4. Apparatus

Electrochemical measurements were performed using a potentiostat/galvanostat (ALS, 660A, CH Instruments Inc.) equipped with a computer. Transmission spectra were recorded on a diode array detection system (USB2000, Ocean Optics). As a reference, a device containing a DMSO-based electrolyte solution dissolved in a supporting electrolyte was used. The surface morphologies of the Ag deposited on the electrodes were examined using FE-SEM (JSM-6510, JEOL) and AFM (SPI3800N & SPA400, SII). The optical properties of the Ag nanoparticles model were calculated by the finite-difference time-domain (FDTD) method (Poynting for Optics, FUJITSU).

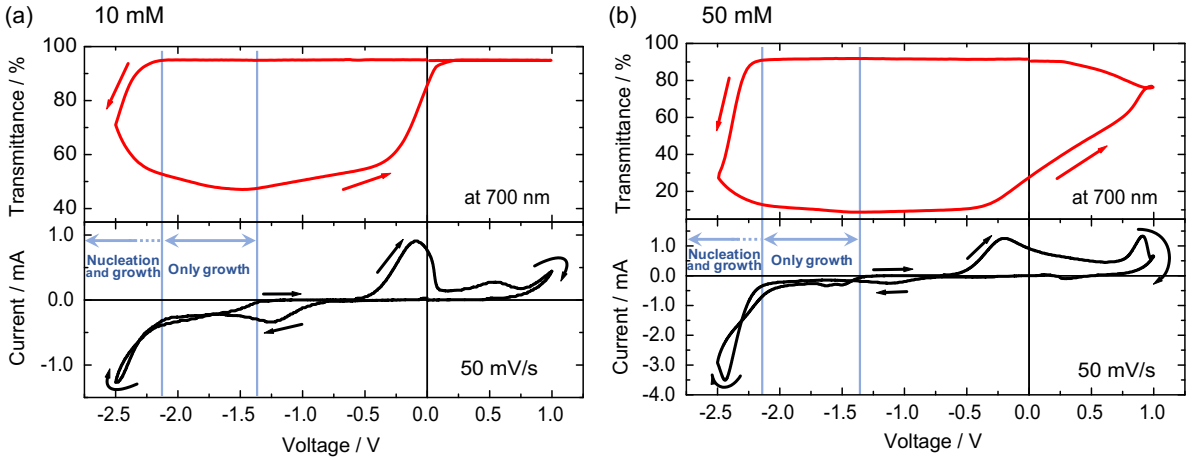


**Fig. 1** Change in transmittance at 700 nm (top) and cyclic voltammogram in a two-electrode system (bottom) of the EC device. The concentration of $Ag^+$ ions are (a) 10 mM (b) and 50 mM. The critical growth voltages determined from the change in current during the voltage sweep for the positive direction and the critical nucleation voltages determined from the decrease of transmittance due to Ag deposition are shown in the graphs with blue lines.

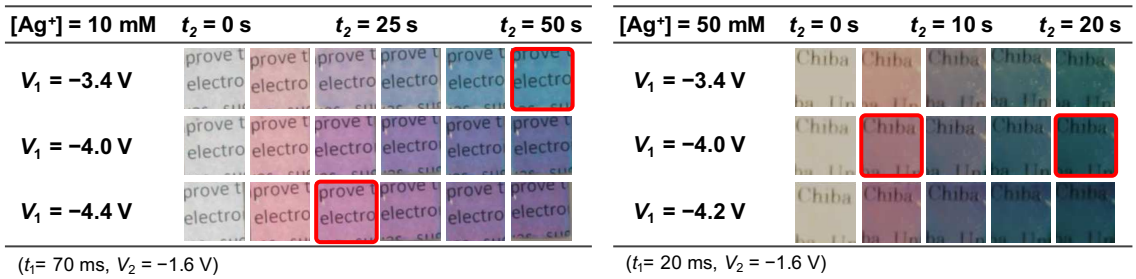


**Fig. 2** Photographs of the EC device taken on a lightbox during voltage application. Left: device containing 10 mM of $Ag^+$ ion. Application sequences were $V_1$ = -3.4, -4.0, or -4.4 V, and $t_1$ = 70 ms, $V_2$ = -1.6 V and $t_2$ = 50 s. Right: device containing 50 mM of $Ag^+$ ion. Application sequences were $V_1$ = -3.4, -4.0, or -4.2 V, and $t_1$ = 20 ms, $V_2$ = -1.6 V and $t_2$ = 20 s.

## 3. Results and discussion

First, the effects of the $Ag^+$ ion concentration in the electrolyte on coloring were investigated. Previously, the concentration was fixed at 50 mM and the concentration dependence was not examined. In this study, the low-concentration electrolyte (10 mM) case is mainly discussed. The cyclic voltammograms and change in transmittance at 700 nm for the two EC devices containing 10 and 50 mM of $AgNO_3$ according to the voltage sweep are shown in Fig. 1. From the cyclic voltammograms and corresponding transmittance changes of the EC devices, the critical voltages required for nucleation and growth of both devices were found to be -2.1 and -1.4 V, respectively. To obtain favorable coloration, step voltage sequences were determined as follows: for the device that contained 10 mM of $Ag^+$ ion, the first voltage was $V_1$ = -3.4, -4.0, or -4.4 V, $t_1$ = 70 ms; the second voltage was $V_2$ = -1.6 V, $t_2$ = 50 s; for the device that contained 50 mM of $Ag^+$ ion, the first voltage was $V_1$ = -3.4, -4.0, or -4.2 V, $t_1$ = 20 ms; the second voltage was $V_2$ = -1.6 V, $t_2$ = 20 s. Photographs of the EC devices during application of second voltages for each first voltage are shown in Fig. 2. For both devices with 10 and 50 mM, the colors were gradually changed from transparent to magenta and cyan during the application of second voltages. More uniform Ag nanoparticles in size and shape enhance the LSPR band sharper; as a result, the device shows a vivid color. According to our previous knowledge, it is considered that the shorter application time of $V_1$ is valid to obtain uniform-sized Ag nanoparticles in this device. However, the $t_1$ for the device containing 10 mM of $Ag^+$ ion was longer than that of other the device (50 mM of $Ag^+$ ion); the former showed a vivid and bright color than the latter (Fig. 2, left and right). This suggests that the concentration of $Ag^+$ ions in the electrolyte largely affects the formation of the deposit. To evaluate the effect of a higher concentration of $Ag^+$ ions on the deposited state, a device containing 150 mM of $Ag^+$ ion was fabricated. The cyclic voltammogram and the corresponding change in transmittance, and photographs of the 150 mM device with application of step-voltage are shown in Figs. S2 and S3. From the cyclic voltammogram, the redox current of the EC device with a higher concentration (150 mM) was considerably larger than that of the EC devices with lower concentrations (10 and 50 mM), suggesting that the rate of supply of $Ag^+$ ions was higher in the case of the 150 mM device. As a result, when the step voltage was applied, the device immediately turned to a the dark color because of the rapid growth of Ag nanoparticles, as shown in Fig. S3. These results suggest the difficulty of precise color control of the device with high $Ag^+$ ion concentration. Thus, this device was not further examined in this study.

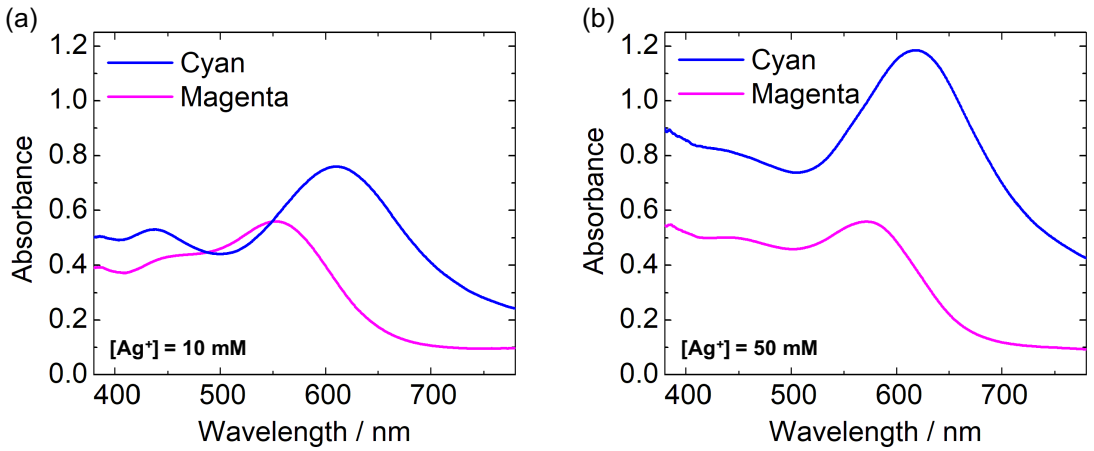


**Fig. 3** Absorption spectra of devices with cyan and magenta colors. (a) Device containing 10 mM of $Ag^+$ ion. Cyan: $V_1$ = -3.4 V, $t_1$ = 70 ms; $V_2$ = -1.6 V, $t_2$ = 50 s. Magenta: $V_1$ = -4.4 V, $t_1$ = 70 ms; $V_2$ = -1.6 V, $t_2$ = 20 s and (b) Device containing 50 mM of $Ag^+$ ion. Cyan: $V_1$ = -4.0 V, $t_1$ = 20 ms; $V_2$ = -1.6 V, $t_2$ = 20 s. Magenta: $V_1$ = -4.0 V, $t_1$ = 20 ms; $V_2$ = -1.6 V, $t_2$ = 5 s.

This suggests that the concentration of $Ag^+$ ions in the electrolyte largely affects the formation of the deposit. To evaluate the effect of a higher concentration of $Ag^+$ ions on the deposited state, a device containing 150 mM of $Ag^+$ ion was fabricated. The cyclic voltammogram and the corresponding change in transmittance, and photographs of the 150 mM device with application of step-voltage are shown in Figs. S2 and S3. From the cyclic voltammogram, the redox current of the EC device with a higher concentration (150 mM) was considerably larger than that of the EC devices with lower concentrations (10 and 50 mM), suggesting that the rate of supply of $Ag^+$ ions was higher in the case of the 150 mM device. As a result, when the step voltage was applied, the device immediately turned to a the dark color because of the rapid growth of Ag nanoparticles, as shown in Fig. S3. These results suggest the difficulty of precise color control of the device with high $Ag^+$ ion concentration. Thus, this device was not further examined in this study.

With $Ag^+$ concentration of 10 mM and 50 mM, the absorption spectra of magenta and cyan states of both devices are shown in Fig. 3. The photograph of the device corresponding to each absorption spectrum is indicated as a red square in Fig. 2. Both magenta colors have peaks at 550 nm, and both cyan colors have peaks at 620 nm and show corresponding colors. The absorbance of the cyan device with 50 mM in the entire visible wavelengths was larger than that with 10 mM, resulting in a dark and dull color, as shown in the photograph (Fig. 2, right).

The lightness ($L^*$) and chroma ($C^*$) values of the devices were calculated from the absorption spectra (Fig. 3) for the above discussed four states (table 1). A CIE standard illuminant D65 was used as the backlight of the device and a CIE 1931 2° standard observer was utilized as a color-matching function. Comparing two cyan states of two different concentration devices, the lightness of the 10 mM device (58.4%) was significantly higher than that of the 50 mM device (42.1%). This suggests that the amount of transmitted light of the 10 mM device was larger than that of the 50 mM device. As for the magenta state, the chroma value of the 10 mM device (20.3) was higher than that of the 50 mM device (9.0), while their lightness values were almost the same. These results suggest that the LSPR band for the magenta representation (around 550 nm) of the 10 mM device clearly appeared compared to that of the 50 mM device.

Then, the morphology of the detailed Ag nanoparticles was precisely investigated by FE-SEM and AFM for the above four states (Fig. 4). Corresponding photographs of the device are also shown in the insets. In the 10 mM device (Figs. 4a, 4c), the deposited Ag nanoparticles were well isolated from each other, and the RMS values evaluated from AFM images were 9.53 nm for cyan and 8.16 nm for magenta. In contrast, for the 50 mM device (Figs. 4b, 4d), Ag nanoparticles suffered coalescence and smooth surfaces were formed. Particularly for cyan, almost all particles were connected and covered the surface of the electrode with a complicated structure, forming a thin layer state. The RMS values were 4.20 nm for cyan and 3.50 nm for magenta, which are lower than that of the 10 mM device.

The differences in the color quality of the devices were considered in terms of morphology of the Ag nanoparticles. Considering cyan states, coalesced Ag deposits show a specular reflection surface and efficiently reflect the incident light[37]. Thus, it was difficult to obtain a cyan state while maintaining its higher lightness. Actually, the grown and coalesced Ag deposits of the 50 mM device seem to block almost all the transmitted light (Fig. 4 (b)). In contrast, for the 10 mM device, the degree of coalescence of the deposited Ag particles was lower than that of 50 mM device, leading to higher transmittance and lightness values, as shown in Table 1. In the case of magenta states of the 10 mM device, improvement of monodispersity and increase in density of the deposited Ag particles would contribute to the appearance of a clear LSPR band, as shown in Fig. 4 (a), resulting in a higher chroma value (Table 1). It was observed that the morphology of the deposited Ag nanoparticles considerably affected the color quality of the EC devices.

**Table 1**. Lightness ($L^*$), a*, b*, and chroma (C*) values in the CIE1976 Lab color space. The values are calculated for six states (cyan, magenta, and yellow in 10 mM and 50 mM devices). The D65 and CIE 1931 2° standard observer were adopted as standard illuminant and color-matching function, respectively.

| | [Ag⁺] | $L^*$ | $a^*$ | $b^*$ | $C^*$ | Voltage condition |
|---|---|---|---|---|---|---|
| Cyan | 10 mM | 58.4 % | −14.0 | −8.2 | 16.2 | $V_1$ = −3.4 V $t_1$ = 70 ms<br>$V_2$ = −1.6 V $t_2$ = 50 s |
| | 50 mM | 42.1 % | −15.6 | −8.3 | 17.7 | $V_1$ = −4.0 V $t_1$ = 20 ms<br>$V_2$ = −1.6 V $t_2$ = 20 s |
| Magenta | 10 mM | 65.1 % | 19.9 | −4.2 | 20.3 | $V_1$ = −4.4 V $t_1$ = 70 ms<br>$V_2$ = −1.6 V $t_2$ = 20 s |
| | 50 mM | 63.8 % | 9.0 | −0.4 | 9.0 | $V_1$ = −4.0 V $t_1$ = 20 ms<br>$V_2$ = −1.6 V $t_2$ = 5 s |
| Yellow | 10 mM | 86.3 % | 4.8 | 22.8 | 23.3 | $V_1$ = −2.6 V $t_1$ = 70 ms<br>$V_2$ = −1.6 V $t_2$ = 200 s |
| Green | 10 mM | 60.1 % | −24.7 | 15.7 | 29.3 | $V_1$ = −2.7 V $t_1$ = 70 ms<br>$V_2$ = −1.6 V $t_2$ = 200 s |

CIE standard illuminant D65, CIE 1931 2° standard observer

It is estimated that such morphological differences come from the density of nuclei generated by $V_1$ applications and the growth rates of particles during $V_2$ applications. The amount of electric charge during $V_1$ application for each device (1.3 mC in the 10 mM device and 1.0 mC in the 50 mM device) was calculated from the change in current shown in Fig. S4. This calculated result indicates that the number of nuclear, namely density of the nuclear per area, was larger for the 10 mM device compared to the 50 mM device.

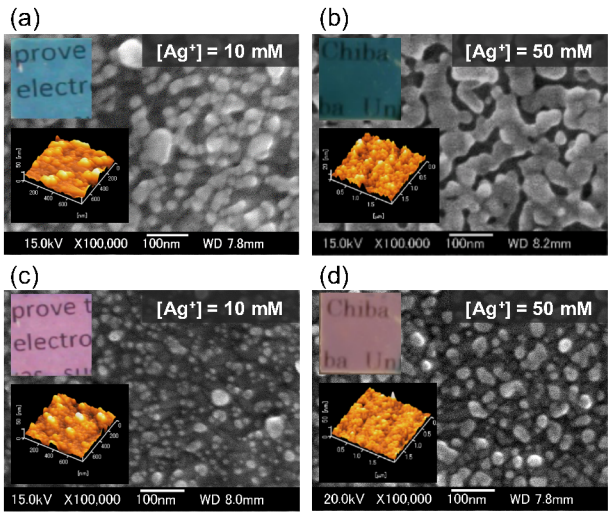


**Fig. 4** FE-SEM and AFM images (insets) of the electrodes surface where Ag particles were deposited. Corresponding photographs of devices are also shown in the insets. (a) Cyan state of the 10 mM device by $V_1$ = -3.4 V, $t_1$ = 70 ms, $V_2$ = -1.6 V, $t_2$ = 50 s. (b) Cyan state of the 50 mM device by $V_1$ = -4.0 V, $t_1$ = 20 ms, $V_2$ = -1.6 V, $t_2$ = 20 s. (c) Magenta state of the 10 mM device by $V_1$ = -4.4 V, $t_1$ = 70 ms, $V_2$ = -1.6 V, $t_2$ = 20 s. (d) Magenta state of the 50 mM device by $V_1$ = -4.0 V, $t_1$ = 20 ms, $V_2$ = -1.6 V, $t_2$ = 5 s.

From the change in currents during $V_2$ applications shown in Fig. 5, it is observed that the current of the 50 mM device (red line) was larger than that of the 10 mM device (black line). These results suggest that a larger number of Ag particles slowly grew during $V_2$ application in the 10 mM device compared to the 50 mM device. This estimation is also in accordance with the observed morphology shown in Fig. 4. In particular, the growth rate of Ag nanoparticles, i.e. reduction current of the $Ag^+$ ions, in the diffusion-limited redox reaction obeys the Cottrell theory. In the theory, the redox current is proportional to the concentration of the reaction agent[46]. That is, after reaching a diffusion-limited redox reaction, the $V_2$ value does not affect the growth rate of Ag nanoparticles. By using a low-concentration device in our case, well-isolated Ag nanoparticles were obtained due to slow growth rate, resulting in preferred colors of cyan and magenta.

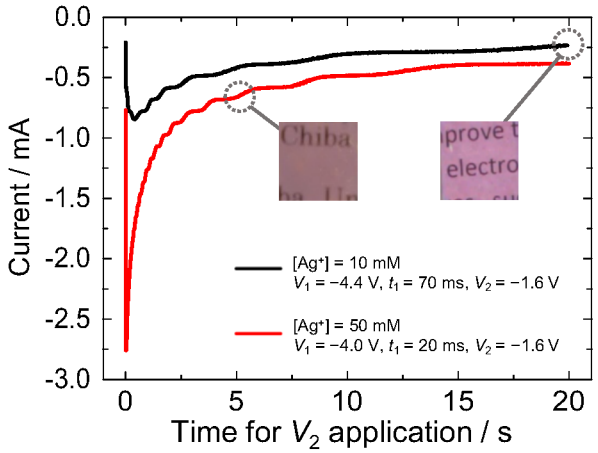


**Fig. 5** Change in currents during $V_2$ application (-1.6 V) when magenta states appear for the devices. The black line shows the device containing 10 mM of Ag ion and the red line shows the device containing 50 mM of Ag ion.

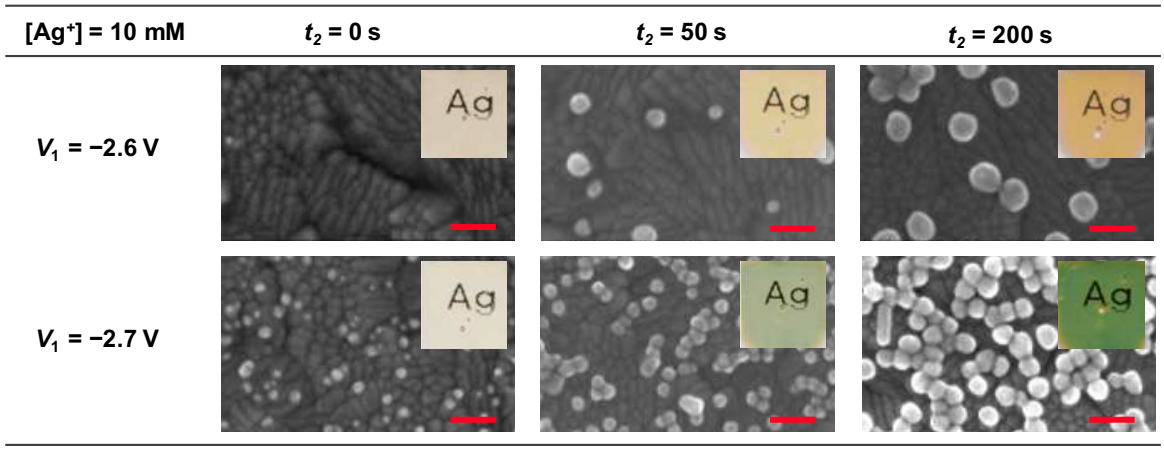


($t_1$= 70 ms, $V_2$ = -1.6 V)

**Fig. 6** FE-SEM images of electrodes surfaces where Ag nanoparticles were deposited and photographs of 10 mM devices (insets) during application of $V_2$ (-1.6 V) after application of $V_1$ (-2.6 or -2.7 V) for 70 ms. All scale bars in red indicate 100 nm.

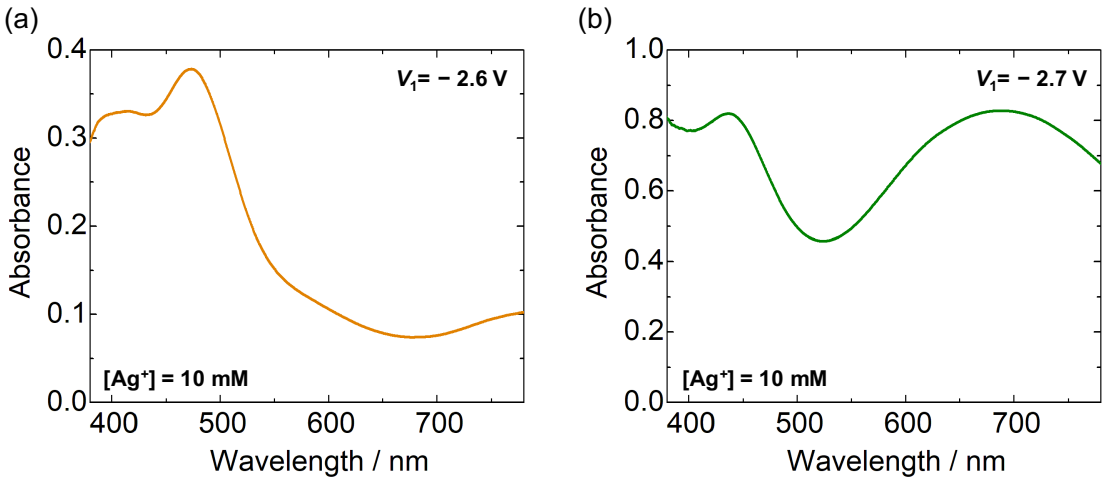


**Fig. 7** Absorption spectra of (a) yellow and (a) green states of the 10 mM device. The sequences of voltage applications were $V_1$ = (a) -2.6 V or (b) -2.7 V, $t_1$ = 70 ms, $V_2$ = 1.6 V, $t_2$ = 200 s.

In sequence, the more formation of uniform Ag nanoparticles, namely spherical Ag nanoparticles existing in isolation, were carried out by utilizing the device containing 10 mM of $Ag^+$ ion. To prevent the connection of Ag nanoparticles, their density, controlled by $V_1$ and $t_1$, should be reduced. Therefore, compared to previous experiments, we determined lower voltages for $V_1$ (-2.6 and -2.7 V). The FE-SEM images and the color changes of the device during the $V_2$ application after $V_1$ application are shown in Fig. 6. The absorption spectra after the $V_2$ application for 200 s under both conditions are also shown in Fig. 7. For the condition $V_1$ = -2.6 V, almost spherical nanoparticles were deposited in isolation from each other and the diameters were ca.70 nm (Fig. 6 top). The device showed a sharp absorption band at approximately 470 nm (Fig. 7 (a)) and exhibited yellow color (Fig. 6 top). In contrast, for the condition $V_1$ = -2.7 V, spherical nanoparticles with diameters of ca. 50 nm were deposited on the electrode in higher density than in the condition $V_1$ = -2.6 V (Fig. 6 bottom). Interestingly, the absorption spectra had two peaks at 437 and 690 nm (Fig. 7 (b)) and the device turned to green (Fig. 6 bottom). In the above-mentioned experiments, which achieved vivid cyan and magenta by applying $V_1$ = -3.4 or -4.4 V, relatively fine and anisotropic nanoparticles were deposited in high density, as shown in Fig. 4. In contrast, by applying lower $V_1$, the morphologies of the Ag nanoparticles changed to a spherical shape and the densities of the deposited nanoparticles were reduced. This reduction in the number of deposited nanoparticles was due to a decrease in the density of the generated nuclei by applying lower nucleation voltages. That is, by decreasing the density of Ag nanoparticles, Ag deposition was controlled by the 3D-diffusion process around Ag nuclei. As $Ag^+$ ions are equally supplied from the electrolyte to all metal particles during $V_2$ application, a more uniform particle growth with a narrow size distribution and formation of spherical particles were successfully achieved.

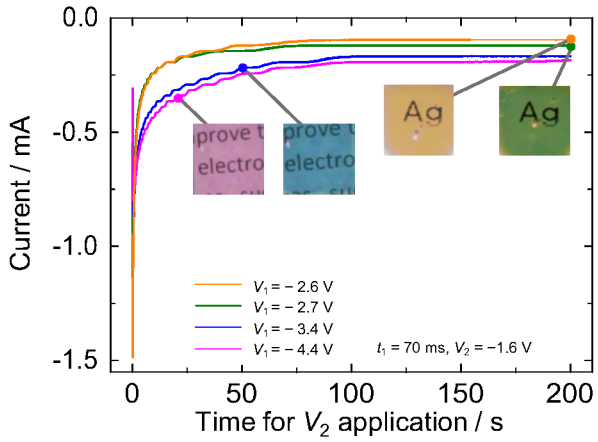


**Fig. 8** Change in currents during application of $V_2$ (-1.6 V) for the 10 mM device after application of four different $V_1$ (-2.6, -2.7, -3.4, or -4.4 V). Photographs in the inset show the device colors at each point.

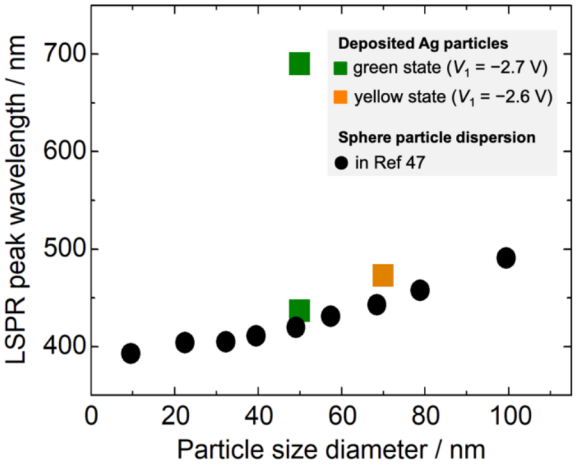


**Fig. 9** LSPR peak wavelength vs. particle size diameter of Ag nanoparticles deposited in the device showing green and yellow states. The reference data for Ag nanoparticles dispersed in aqueous suspensions are plotted from previous publications[45].

Cathodic currents under $V_2$ application, namely the rates of supplying $Ag^+$ ions to Ag nanoparticles on the electrode per unit of time, decreased according to the positive shift of $V_1$, as shown in Fig. 8. This result indicates that the nucleation voltage of $V_1$ affects the subsequent growth of Ag nanoparticles under $V_2$ application.

Then, the difference of electrodeposition behavior of Ag nanoparticles between $V_1$ = -2.6 and -2.7 V (Fig. 6 top and bottom) was also considered in terms of nuclear density, generated in $V_1$ stage. In the case of $V_1$ = -2.6 V, the number of nuclei was limited to small numbers, and finally spherical particles were obtained in almost isolation. These isolated spherical Ag nanoparticles are yellow in color, as shown in the inset photo (Fig. 6). The yellow coloration caused by Ag electrodeposition on the smooth ITO surface has not been reported. In a previous study[37], fine (diameter of 10–20 nm) and isolated Ag nanoparticles with yellow color were deposited by utilizing a porous electrode modified with ITO nanoparticles. When $V_1$ = -2.7 V was applied, the number of nuclei was slightly increased compared to that when -2.6 V was applied, leading to connected spherical particles with relatively high density. This spherical morphology of the Ag deposit might be the cause of the green coloration shown in Fig. 6. In particular, the green-colored device showed two distinct absorption bands, as shown in Fig. 7(b).

These spherical Ag nanoparticles with yellow or green color were more considered in terms of LSPR wavelength. The absorption bands of the devices were due to the LSPR bands induced by Ag nanoparticles. The relationship between the average diameter of Ag nanoparticles measured from SEM images and the LSPR peak wavelength of the device with yellow and green colors, by applying $V_2$ for 200 s, are plotted in Fig. 9. The relationship between the diameter of spherical Ag nanoparticles and the LSPR peaks in aqueous dispersion[47] are also illustrated by the black circles in Fig. 9. As mentioned in our previous research[37], the LSPR peak enhanced by spherical Ag nanoparticles electrochemically generated in the EC device significantly coincide with that of spherical Ag particles dispersed in solution when the diameters are the same. In this research, 70 nm of spherical Ag nanoparticles showed a yellow state with absorption peak of 473 nm. This almost met the tendency for the LSPR peak wavelength of dispersed spherical Ag nanoparticles. As for the green color state, the LSPR peak at a short wavelength (437 nm) met the tendency of the dispersion. The absorption peak at a longer wavelength (690 nm) could be due to the dramatic shift of the LSPR band by the coupling of a number of particles. Incidentally, in spite of these small diameters, for the cyan or magenta states the LSPR bands were in the long-wavelength range. These colorations were due to the effect of the anisotropic structures or fusion between particles, as previously reported[36,37].

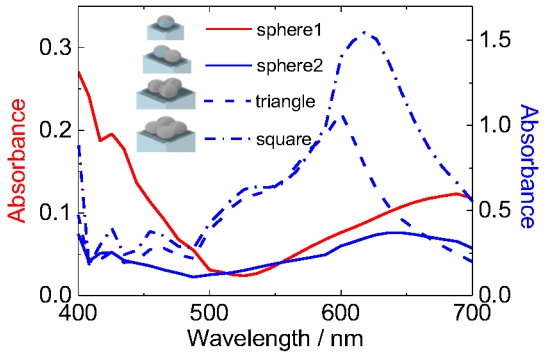


**Fig. 10** Calculation results of absorption spectra of arrayed Ag spherical particles with a particle diameter of 50 nm using the FDTD method. Four models are illustrated next to the graph legends.

To discuss the specific LSPR spectrum of the green-colored device, the effects of the connection of Ag nanoparticles on the LSPR wavelength and the absorption spectra of arrayed spherical Ag particles of 50 nm in size were calculated by the FDTD method (Fig. 10). The four models illustrated in Fig. 10 were calculated. The model "sphere 1" represents the state in which Ag nanoparticles were deposited in isolation. The models "sphere2", "triangle", and "square" represent the state in which 2-4 Ag particles were connected, as

shown in the illustrations. The "sphere 1" showed a single LSPR band in the wavelength range of 400–500 nm, which was in accordance with that of the spherical Ag nanoparticles dispersion. In contrast, new LSPR bands appeared in the wavelength range of 600–700 nm for the other models. These results indicate that the absorption peaks in the longer wavelength region in the green-colored device resulted from the enhancement of LSPR by connected Ag particles of 50 nm.

## 4. Conclusion

In this study, we aimed to improve the color quality of the Ag deposition-based multicolor EC devices by precisely controlling the supply of $Ag^+$ ions to the electrode surface. Initially, the effect of coloration by decreasing the concentration of $Ag^+$ ions in the Ag deposition-based EC device was investigated. As a result of optimizing the driving voltage, a lower concentration device (10 mM $Ag^+$ ion) showed vivid and bright colors of cyan and magenta.

This improvement was due to the generation of fine Ag nanoparticles and prevention of the connection of Ag particles. From the electrochemical investigation, it was suggested that the slow supply rate of $Ag^+$ ions in the lower concentration device induced electrochemical deposition of fine and isolated Ag nanoparticles.

In sequence, to obtain more uniformly deposited Ag nanoparticles, the nucleation voltage of $V_1$ was set to a lower voltage in the 10 mM device. As a result, spherical Ag nanoparticles were successfully obtained, and the device showed yellow and green colors. By comparing the LSPR behavior of the device with that of Ag nanoparticles dispersed in solution and using FDTD calculations, the mechanism of the yellow and green colors was investigated in detail. Thus, it was indicated that the yellow coloration with an absorption band in the 400-500 nm region was caused by LSPR absorption of isolated spherical Ag nanoparticles. Furthermore, it was also observed that the coexistence of isolated spherical particles and aggregations of Ag nanoparticles induced two types of LSPR bands, leading to good green color.

By precisely controlling the supply of $Ag^+$ ions in the device, four chromatic colors (cyan, magenta, yellow, and green) were successfully achieved on a flat ITO electrode, that is, the EC device was the simplest structure of two flat ITO electrodes and a sandwiched EC solution. The EC device in this constitution realize not only such a chromatic color but also black or mirror state. In addition, it has the ability to switch its optical state a few thousand times according to the stable reaction of the deposition and dissolution of Ag[35]. Such a high stability is desirable for practical application. It can also be utilized as a display device in the same way as other EC devices by using a pattern-printed electrode or by driving a matrix.[48] Therefor, it is expected that the development of LSPR based EC devices will gradually accelerate in the near future based on these research results or investigation methods and to be utilized for next-generation smart windows or display devices.

## Conflicts of interest

There are no conflicts to declare.

## Acknowledgements

This work was partly supported by JSPS KAKENHI (17H06377, 15H03880, and 19J21962) and JST A-STEP (AS2915036S).

## References

1 P. Monk, R. Mortimer and D. Rosseinsky, *Electrochromism and Electrochromic Devices*, Cambridge University Press, Cambridge, 2007.
2 D. R. Rosseinsky and R. J. Mortimer, *Adv. Mater.*, 2001, **13**, 783–793.
3 Y. Kondo, H. Tanabe, H. Kudo, K. Nakano and T. Otake, *Materials (Basel).*, 2011, **4**, 2171–2182.
4 N. Kobayashi, S. Miura, M. Nishimura and H. Urano, *Sol. Energy Mater. Sol. Cells*, 2008, **92**, 136–139.
5 D. Corr, U. Bach, D. Fay, M. Kinsella, C. McAtamney, F. O'Reilly, S. N. Rao and N. Stobie, *Solid State Ionics*, 2003, **165**, 315–321.
6 H. Urano, S. Sunohara, H. Ohtomo and N. Kobayashi, *J. Mater. Chem.*, 2004, **14**, 2366–2368.
7 C. M. Lampert, *Mater. Today*, 2004, **7**, 28–35.
8 A. Azens and C. G. Granqvist, *J. Solid State Electrochem.*, 2003, **7**, 64–68.
9 G. A. Niklasson and C. G. Granqvist, *J. Mater. Chem.*, 2007, **17**, 127–156.
10 K. Wang, H. Wu, Y. Meng, Y. Zhang and Z. Wei, *Energy Environ. Sci.*, 2012, **5**, 8384–8389.
11 A. S. Ribeiro, V. C. Nogueira, P. Faria dos Santos Filho and M. A. De Paoli, *Electrochim. Acta*, 2004, **49**, 2237–2242.
12 S. H. Hsiao and Y. Z. Chen, *Eur. Polym. J.*, 2018, **99**, 422–436.
13 Z. Liang, K. Nakamura and N. Kobayashi, *Sol. Energy Mater. Sol. Cells*, 2019, **200**, 109914.
14 R. J. Mortimer, *Electrochim. Acta*, 1999, **44**, 2971–2981.
15 R. Neskovska, M. Ristova, J. Velevska and M. Ristov, *Thin Solid Films*, 2007, **515**, 4717–4721.
16 X. H. Xia, J. P. Tu, J. Zhang, X. L. Wang, W. K. Zhang and H. Huang, *Sol. Energy Mater. Sol. Cells*, 2008, **92**, 628–633.
17 K. R. Reyes-Gil, Z. D. Stephens, V. Stavila and D. B. Robinson, *ACS Appl. Mater. Interfaces*, 2015, **7**, 2202–2213.
18 S. H. Lee, R. Deshpande, P. A. Parilla, K. M. Jones, B. To, A. H. Mahan and A. C. Dillon, *Adv. Mater.*, 2006, **18**, 763–766.
19 K. Ho Kim, *Int. J. Electrochem. Sci.*, 2020, **15**, 4065–4071.
20 Y. Ren, T. Fang, Y. Gong, X. Zhou, G. Zhao, Y. Gao, J. Jia and Z. Duan, *J. Mater. Chem. C*, 2019, **7**, 6964–6971.
21 I. Mjejri, A. Rougier and M. Gaudon, *Inorg. Chem.*, 2017, **56**, 1734–1741.
22 J. Wang, L. Zhang, L. Yu, Z. Jiao, H. Xie, X. W. (David) Lou and X. Wei Sun, *Nat. Commun.*, 2014, **5**, 4921.
23 Z. Bi, X. Li, Y. Chen, X. He, X. Xu and X. Gao, *ACS Appl. Mater. Interfaces*, 2017, **9**, 29872–29880.
24 M. Ishizaki, H. Ando, N. Yamada, K. Tsumoto, K. Ono, H. Sutoh, T. Nakamura, Y. Nakao and M. Kurihara, *J. Mater. Chem. A*, 2019, **7**, 4777–4787.
25 T. C. Liao, W. H. Chen, H. Y. Liao and L. C. Chen, *Sol. Energy Mater. Sol. Cells*, 2016, **145**, 26–34.

26 K. M. Lee, H. Tanaka, A. Takahashi, K. H. Kim, M. Kawamura, Y. Abe and T. Kawamoto, *Electrochim. Acta*, 2015, **163**, 288–295.
27 K. Moo Lee, H. Tanaka, K. Ho Kim, M. Kawamura, Y. Abe and T. Kawamoto, *Appl. Phys. Lett.*, 2013, **102**, 2011–2014.
28 C. Park, S. Seo, H. Shin, B. D. Sarwade, J. Na and E. Kim, *Chem. Sci.*, 2015, **6**, 596–602.
29 X. Hou, Z. Wang, Z. Zheng, J. Guo, Z. Sun and F. Yan, *ACS Appl. Mater. Interfaces*, 2019, **11**, 20417–20424.
30 Y. Yue, H. Li, K. Li, J. Wang, H. Wang, Q. Zhang, Y. Li and P. Chen, *J. Phys. Chem. Solids*, 2017, **110**, 284–289.
31 S. M. Cho, S. Kim, T.-Y. Kim, C. S. Ah, J. Song, S. H. Cheon, J. Y. Kim, H. Ryu, Y.-H. Kim, C.-S. Hwang and J.-I. Lee, *Sol. Energy Mater. Sol. Cells*, 2018, **179**, 161–168.
32 K. R. Jeong, I. Lee, J. Y. Park, C. S. Choi, S. H. Cho and J. L. Lee, *NPG Asia Mater.*, , DOI:10.1038/am.2017.25.
33 S. I. Córdoba De Torresi and I. A. Carlos, *J. Electroanal. Chem.*, 1996, **414**, 11–16.
34 A. L. S. Eh, M. F. Lin, M. Cui, G. Cai and P. S. Lee, *J. Mater. Chem. C*, 2017, **5**, 6547–6554.
35 S. Araki, K. Nakamura, K. Kobayashi, A. Tsuboi and N. Kobayashi, *Adv. Mater.*, 2012, **24**, OP122–OP126.
36 A. Tsuboi, K. Nakamura and N. Kobayashi, *Adv. Mater.*, 2013, **25**, 3197–3201.
37 A. Tsuboi, K. Nakamura and N. Kobayashi, *Chem. Mater.*, 2014, **26**, 6477–6485.
38 R. Onodera, A. Tsuboi, K. Nakamura and N. Kobayashi, *J. Soc. Inf. Disp.*, 2016, **24**, 424–432.
39 A. Tsuboi, K. Nakamura and N. Kobayashi, *Sol. Energy Mater. Sol. Cells*, 2016, **145**, 16–25.
40 S. Kimura, K. Nakamura and N. Kobayashi, *Sol. Energy Mater. Sol. Cells*, 2020, **205**, 110247.
41 D. D. Evanoff and G. Chumanov, *J. Phys. Chem. B*, 2004, **108**, 13957–13962.
42 T. Huang and X. H. N. Xu, *J. Mater. Chem.*, 2010, **20**, 9867–9876.
43 E. Kazuma, T. Yamaguchi, N. Sakai and T. Tatsuma, *Nanoscale*, 2011, **3**, 3641–3645.
44 M. Ueda, H. Dietz, A. Anders, H. Kneppe, A. Meixner and W. Plieth, *Electrochim. Acta*, 2002, **48**, 377–386.
45 G. Sandmann, H. Dietz and W. Plieth, *J. Electroanal. Chem.*, 2000, **491**, 78–86.
46 N. Serizawa, Y. Katayama and T. Miura, *Electrochim. Acta*, 2010, **56**, 346–351.
47 D. Paramelle, A. Sadovoy, S. Gorelik, P. Free, J. Hobley and D. G. Fernig, *Analyst*, 2014, **139**, 4855–4861.
48 A. Tsuboi, K. Nakamura and N. Kobayashi, *J. Soc. Inf. Disp.*, 2013, **21**, 361–367.

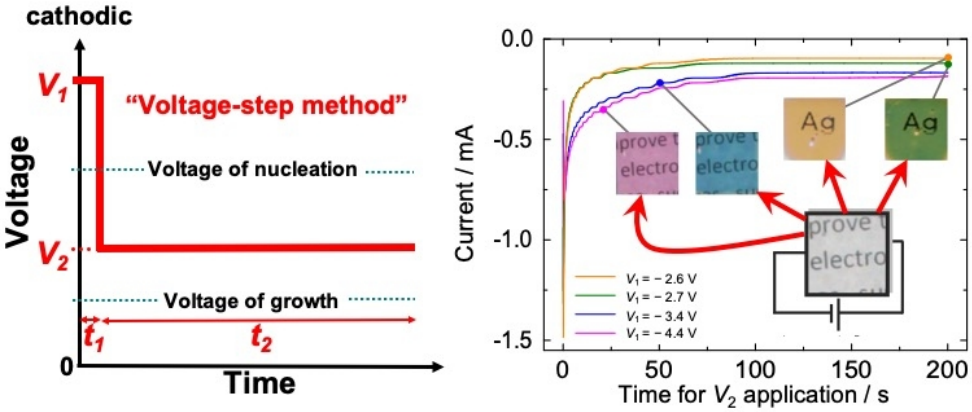


271x117mm (72 x 72 DPI)